

Informatik-Bericht Nr. 2008-6

Schriftenreihe Fachbereich Informatik, Fachhochschule Trier

Advanced Methods for Target Navigation using Microelectrode Recordings in Stereotactic Neurosurgery for Deep Brain Stimulation

Peter Gemmar, Oliver Gronz, Thorsten Henrichs
University of Applied Sciences (FH) Trier
Institute for Innovative Informatics Applications i3A
Schneidershof, 54293 Trier, Germany
p.gemmar@fh-trier.de

Frank Hertel
Klinikum Idar-Oberstein GmbH
Dr. Ottmar-Kohler-Str. 2
55743 Idar-Oberstein, Germany
f.hertel@shg-kliniken.de

Abstract

This study describes novel methods for navigating and placing of electrodes into specific structures in the basal ganglia for deep brain stimulation (DBS), as it is common in the treatment of Parkinson's disease. Critical to these procedures in neurosurgery is the localization and identification of different target structures such as subthalamic nucleus (STN) along the electrode's trajectory and finding the best position for the stimulating electrode.

Typically, microelectrode recordings (MER) of local neural activity along up to five parallel trajectories are used by neurosurgeons for detecting the target region and creating the anatomic positions of the electrodes by imagination. We developed a method for automatic classification of the MER signals, which provides an electrode model with patient specific borders of the STN. In addition, a method is provided for finding the best matching of the electrode model with a 3D model of the STN. As a result, a 2.5D visualization of the target region is produced with the most probable positions of the electrodes and their intersections.

1. Introduction

Stereotactic deep brain stimulation (DBS) is a widespread treatment option for different kinds of neurological diseases, especially movement disorders, such as Parkinson's disease (PD), Dystonia, different kinds of tremors, or chronic pain also [1]. In the treatment of advanced PD the subthalamic nucleus (STN) is considered the most promising target. The STN is a small, almond-shaped structure of approx. 0.6 ml, which is located in the midbrain, adjacent to the Substantia Nigra and the red nucleus [2].

The anatomical localization of the STN as target for stimulation is the primary task in the stereotactic planning

phase. T1-weighted magnetic resonance images (MRI) are used for extracting the target points and planning of safe trajectories for moving the electrodes to these targets. This task can be performed automatically using image processing algorithms [3]. However, the STN cannot be identified in T1-MRI which are actually available. And because T2-weighted MRI bear geometric inhomogeneities, the target points are determined indirectly from the positions of the anatomical landmarks anterior (AC) and posterior (PC) commissure of the 3rd ventricle which can be well detected in T1-MRI. The initial target coordinates for the STN are approximated by a fixed and commonly used 3D distance from the midcommissural point [4]. Obviously, these coordinates deviate from the patient's real STN coordinates.

In the surgery phase a stereotactic frame is used for pushing the stimulating electrodes – one per each hemisphere – towards the target points. However, MRI distortions, limited mechanical precision, shifting of the brain within the cranium, and the aforementioned coordinate approximation prevent from reaching precisely the real target structure with the electrode's stimulation poles. It must not be stressed extra, that a procedure with highest placing precision should ensure better therapy results and reduce side effects. For this reason, two measures can be taken interoperatively to assure therapy success. First, up to five electrodes are inserted on parallel trajectories for finding the best hit with the target structure. Second, most surgeons use microelectrode recordings (MER) to locate the target structure. MER signals measure the local activity within a small area proximal to the tip of the electrode as it is moved stepwise through the patients's brain. The MER of different brain structures can be distinguished by experienced neurophysiologists considering commonly known features such as background activity, spike or burst rates [5, 6].

Classification of the MERs is sometimes ambiguous even for experienced neurosurgeons. There are different approaches for automatic analysis and classification of

MER signals using statistical features or digital spike trains [7, 8, 9]. In the following we introduce a method for MER classification based on soft-denoising and multi-level decomposition of the MER signals. The method extracts features for a multi-level geometric classifier independent from specific patient characteristics.

As a result of MER classification – either manually or automatically – the sections for each electrode’s trajectory are labeled, which pass through the STN. The neurosurgeon can use this information to create a geometric association of the labeled sections with the anatomic shape of the STN by imagination. Now, having the seeming positions of the electrodes in mind, the neurosurgeon can estimate the real target location and finally determine the position of the stimulating electrode.

Up to now, the geometric reference of the target structure is commonly taken from atlas data [10, 11], and a generalized shape is mainly considered together with more or less anatomical alterations related to age or disease. If it is possible to extract the physiological description of the STN from T2-MRI or next generation T1-MRI (other target structures are already feasible), a model of the labeled electrodes could be matched with patient specific target information. By this means, a better and patient specific localization and placing of electrodes will be provided.

We have developed a method for matching of electrode models generated from automatic MER labeling with geometric models of the target object. The latter could be a generalized object model or a 3D STN object individually extracted from T1- or T2-MRI. The intraoperative fusion of MER data with MRI or model data facilitates a better navigation of the stimulating electrodes. One direct outcome of the procedure is a 2.5D visualization of the target object with inserted and intersecting electrodes. Hereby, the neurosurgeon gets an objective and illustrative aid for positioning of the stimulating electrode.

2. Materials and methods

MERs for classifier development and testing were recorded using microelectrodes, microdrive and Leadpoint™ from Medtronic Inc. They were recorded at the Hospital of the Merciful Brethren in Trier, Germany. The sampling rate of all MERs is $24kHz$, the signal length is 10s. MER signals were measured in 1 mm (0.5 mm in target proximity) intervals along the electrode’s trajectory.

For matching of the labeled MERs data with the target structure we used 3D object models of the STN. Two types of models were considered: a synthetic STN model of ellipsoidal shape and a discrete volume image of which each STN voxel was manually segmented from T2-weighted MRI with 0.86 mm pixel spacing and 1.6 mm slice thickness.

2.1. Signal properties of STN

Within the last decade, main characteristics for identifying MER signals from STN have been discussed and described thoroughly (e.g. [5] and [6]). Accordingly, the most promising criteria for recognition of STN signals are the distribution of spikes and bursts and an increased background noise (Fig. 1 and 2). However, published measure-

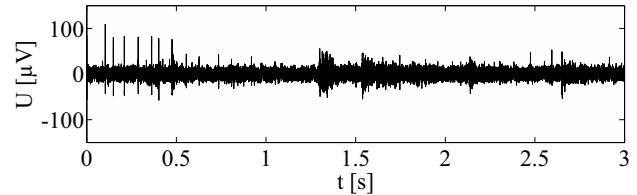


Figure 1. MER without neuronal activity

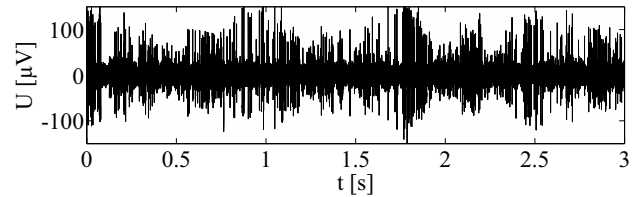


Figure 2. MER of STN neurons

ments of features like spike rate and spike distribution differ significantly, which seems to be natural, as these values differ from person to person.

A typical trajectory might intersect the overlying zona incerta before the electrode reaches STN and finally the underlying substantia nigra (SNr). As up to five electrodes are used, at least two or three electrodes will show STN signals.

Benazzouz et. al. [5] describe the signals vividly: “During a typical exploratory track, we can observe a very low background noise in the zona incerta and almost complete absence of single cell recording. Penetration of the electrode tip into the STN is characterized by a sudden increase in background activity and single cell activity of spontaneously active neurons. The exit of electrode tip out of the STN corresponds to a decrease in background noise and a loss of single cell activity. Spontaneous neuronal activity increases again when the electrode tips enter the substantia nigra pars reticulata (SNr);”

In addition, the pattern of single cell activity in the SNr is a more regular tonic activity while STN cells exhibit an irregular or bursty firing pattern. Hutchison [6] describes a mean firing rate inside STN of $37 \pm 17spikes/s$, for SNr $71 \pm 23spikes/s$. Benazzouz [5] measured $42.3 \pm 22spikes/s$ for STN. Obviously, there is no global threshold to distinguish between STN and SNr. For some patients,

the firing rate of SNr might be lower than STN's firing rate of other patients or vice versa.

2.2. Classifier architecture

Our classifier consists of three levels. Each of these levels decides whether a specific criterion is fulfilled or not. First MER signals from potential neuronal active areas – and the according depth on the electrode path – are marked. In the second step, those marked signals are inspected with respect to the irregular bursting pattern of STN. A key element of this step is the usage of wavelets to de-noise signals and to describe only specific frequency ranges. In some cases, several depth intervals along the electrode path are classified as STN signals according to the second level. Those multiple intervals are handled by the third step that examines the spike distribution.

The complete procedure works without general thresholds concerning spike distribution or firing rate. All MER signals of one electrode are inspected together and patient-specific thresholds are determined automatically.

2.3. Level 1 - finding neuronal sections

Single MER signals can be represented by a vector s . For one electrode, n MER signals are recorded giving signals $s_i, 1 \leq i \leq n$. $s_{i,j}$ describes the j -th discrete sample of recording s_i .

In this level, potential neuronal active MER signals are marked using background activity as the decision criterion. Two different thresholds are determined. The first threshold ϑ_{med} is calculated by

$$\vartheta_{med} = \frac{\sum_{i=1}^n \text{median}(|s_i|)}{n} \cdot c \quad (1)$$

and the second threshold is the mean standard deviation of all MERs increased by a global and static scaling factor c :

$$\vartheta_{std} = \frac{\sum_{i=1}^n \sigma_i}{n} \cdot c \quad (2)$$

In the next step, each s_i is subdivided into n_1 intervals with a length of $10/n_1 \|s_i\|_2$. For each interval, the standard deviation and the median of absolute values are calculated.

The intervals that exceeded ϑ_{med} are counted and the ratio of this number to the total number of intervals is calculated. This result is stored in a vector of length n , where each element represents the ratio of one signal s_i . Accordingly, the same is done for those intervals that exceed ϑ_{std} . Finally, the two vectors are combined by calculating the mean element by element.

Now, let I be the set of indices of signals s_i that were identified as coming from neuronal active areas. Unfortunately, all $i \in I$ are not necessarily connected: several sub-

sets of recordings can belong to I where other recordings $s_j, j \notin I$ were measured in depths between.

2.4. Signal preprocessing for level 2 and 3

The following two levels of the classifier concentrate on the number of spikes and their distribution. To handle the spikes in an optimal manner, the background activity should be removed as far as possible. In addition certain components of this signal are extracted using multilevel 1-D wavelet decomposition. This transformation results in a set of coefficients which is the actual input of level 2 and 3.

2.4.1. De-noising by soft-thresholding. We can assume that two different sources are responsible for the background activity: first the activity of a large set of neurons in different distances to the electrode and second noise produced by the recording system itself, which is present for signals outside STN, too.

Concentrating on the first source, the signal s_i respectively each sample $s_{i,j}$ is a sum of strong single cell activity of spontaneously active neurons close to the electrode, which produces the so-called spikes, and activity of a large set of neurons firing independently and in random manner. Thus, the samples $s_{i,j}$ can be approximated as a sum of single cell activity $\hat{s}_{i,j}$ and independent and identically distributed standard Gaussian random variables z_j

$$s_{i,j} = \hat{s}_{i,j} + z_j, i = 1, \dots, n, j = 1, \dots, m \quad (3)$$

The noise produced by the recording system can be described similarly.

To remove this kind of noise or to estimate the unknown signal \hat{s}_i "De-noising by Soft-Thresholding" [12] is an effective tool. The result \tilde{s}_i of this estimator fullfills two different criteria. Firstly, with high probability \tilde{s}_i is at least as smooth as \hat{s}_i and secondly, the estimator comes nearly as close in mean square to \hat{s}_i as any measurable estimator can come to (according to [12]).

Signal s_i is transformed to wavelet domain resulting in a set of coefficients $(c_k)_{k \in J}$. A threshold τ is determined and the set is transformed using this soft threshold (eq. 5). Finally, the modified coefficients $(\tilde{c}_k)_{k \in J}$ are transformed back to time domain, resulting in the estimation \tilde{s}_i .

Wavelet transformation [13] is one way to describe a signal s as a linear combination

$$s = \sum_{k \in J} c_k \psi_k \quad (4)$$

where $(\psi_k)_{k \in J}$ is a set of orthonormal basis functions and J is a finite set of indices.

$$\tilde{c}_k := \begin{cases} 0 & \text{if } |c_k| \leq \tau \\ \text{sign}(c_k)(|c_k| - \tau) & \text{if } |c_k| > \tau \end{cases} \quad (5)$$

Fig. 3 shows the result of the de-noising process. The background activity contained in the original signal (Fig. 2) is nearly completely removed and only the spikes remain.

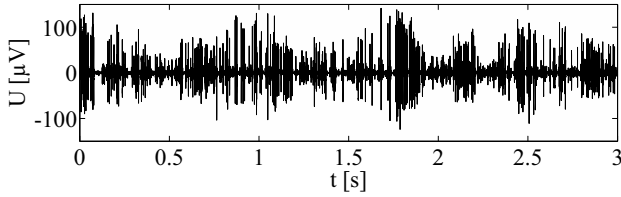


Figure 3. Signal after noise reduction

2.4.2. Multilevel 1-D wavelet decomposition. Multilevel 1-D wavelet decomposition can be compared to a microscope: \tilde{s}_i can be viewed with any desired scaling (magnification) at any point in time.

In each level of the process, the signal is split into two parts. One part is convolved with a high-pass ϕ_{high} followed by dyadic decimation (downsampling) resulting in the detail coefficients cD_1 of level 1. The other part is convolved with a low-pass ϕ_{low} followed by dyadic decimation resulting in the approximation coefficients cA_1 of level 1. The latter ones are used as input for level 2, resulting again in detail coefficients cD_2 respectively in approximation coefficients cA_2 that are used for the next level etc.

2.5. Level 2 - identifying STN signals

STN single cell activity is characteristically described as irregular or bursty. Level 2 of the classifier uses the detail coefficients cD_3 to decide whether a signal s_i is STN or not. We can assume that cD_3 only contains spikes of single cell activity (more or less). A single coefficient from cD_3 has a high value, if a spike with great amplitude is contained at the corresponding point in time in s_i ; low values represent the absence of spikes.

In order to identify those signals with variances changing over the time each coefficient vector $cD_{3,i}$ of the corresponding signal $s_i, i \in I$ is subdivided into n_2 intervals. The difference between smallest and largest variance of the intervals of each $cD_{3,i}, i \in I$ are calculated. All the differences of the used $cD_{3,i}, i \in I$ are considered for determining a threshold. Finally, a new set of indices K is created: each $s_k, k \in K$ exceeds this threshold. Therefore, the signals, the variance of which changes in time, are contained in this index set.

2.6. Combining results of level 1 and 2

From the whole set of signals, two index sets I and K are available. I represents those signals that are neuronal

active according to level 1; K contains those signals that show irregular, bursty behaviour. Furthermore, we know that $K \subset I$ holds.

At first, we look at signals $s_i, i \in I$. They can be partitioned in different index intervals with signals $s_j, j \notin I$ in between: $s_{i_1..s_{i_2}}, s_j, s_{i_3..s_{i_4}}$ where $i_1 \leq i_2 < i_3 \leq i_4; i_1, i_2, i_3, i_4 \in I$ and $i_2 + 1 < i_3$. As the increased background activity is a major criterion for STN activity, all index intervals are labeled as STN which were marked in level 1 and contain at least one signal $s_k, k \in K$. For most electrodes, only one interval will fulfill this criterion and this interval corresponds to the one classified as STN by the surgeon. Table 1 contains an artificial example where different combinations of the level's outcomes are shown and combined.

Index	1	2	3	4	5	6	7	8	9	10	11	12
Result 1st level	N	S	S	S	N	S	S	N	N	S	S	N
Result 2nd level	N	N	S	S	N	N	N	N	N	S	N	N
Combination	N	S	S	S	N	N	N	N	N	S	S	N

S represents STN signals - N represents non-STN signals.

Table 1. Example for combination of results

2.7. Level 3 - removing multiple areas

In some rare cases, the result vector will contain several intervals that were classified as STN according to level 1 and 2. Usually, one interval might be STN, the other interval SNr. and according to the order of occurrence the SNr signals will have higher indices.

To distinguish the erroneously classified signals, the spike rate or the depth can be used. The latter criterion is easy to implement. Using the spike rate as a criterion makes the revision of a STN classification more complex. For it, the distribution of the coefficient values is examined for each vector $cD_{3,i}$. We define n_3 intervals over the range $max(cD_{3,i})$ of coefficient values from all coefficient vectors ($i \in I$). Then, the distribution of the coefficient values is calculated with respect to the value intervals, giving us n_3 bins for each vector $cD_{3,i}$. As some signals might contain outliers produced by the recording system, the ranges of the n_3 value intervals are decreased by a linear factor until the bin of the topmost interval counts at least for 10 coefficients.

Finally, the distribution of the coefficients is inspected using several conditions. If the bins are distributed equally over all intervals, the signal will not contain distinctive spikes and the classification of this recording can be revised. The result is also revised, if the count in the higher bins is big: this recording is probably SNr. In Table 1, the signals s_2, s_3 and s_4 belong to one interval, signals s_{10} and s_{11} belong to another one.

2.8. Fusion of electrode and object models

Labeled MER signals provide basic hints about the real position of the microelectrodes within the target structure. A geometric interpretation of this information requires the combination with further information about the anatomy of the STN (from atlases or from patient specific MRI) and estimated optimal intersections of the electrodes with the target structure STN. This is a critical task for the neurosurgeon, and it doesn't become easier if one takes in account all the known and possible distortions of data.

The real position of the electrodes related to the target object can be estimated by geometrically matching a model of the labeled electrodes with a model of the target structure, and then examining all possible configurations of one with the other. Searching for an optimal configuration of the models can be performed under restrictions, since the orientation of the electrodes is known and possible displacements of the related object are limited. We have developed an algorithm for finding the geometric position where the labeled electrodes intersect the target object in an optimal manner. Visualization of the estimated positions of electrodes in conjunction with the target volume (STN) should facilitate and standardize the decision for the final placement of the electrode.

2.8.1. Object modeling and matching. The representation of the electrodes should describe the geometric position of the labeled intervals (STN or non-STN) along the trajectories, and it should also support easy calculation of their intersections with the object surface. We use a vectorized description of a straight line representing the electrode's trajectory. Let us assume, that we have five parallel electrodes arranged like five spots on a dice with a distance of 2 mm between the outer electrodes and the center electrode. We further know, that the center electrode hits the planned target point, which we denote by vector \vec{x}_t . Let \vec{x}_e be the vector of the point where the center electrode enters into STN. Then straight line l describes all points lying on the center electrode:

$$l : \vec{x} = \vec{x}_t + d \cdot (\vec{x}_t - \vec{x}_e) \quad , \quad (6)$$

where d is a parameter representing the depth and $d = 0$ holds for the target point. For simplification we define the direction vector \vec{x}_d by

$$\vec{x}_d = \frac{\vec{x}_t - \vec{x}_e}{\|\vec{x}_t - \vec{x}_e\|_2} \quad . \quad (7)$$

Now, the remaining electrodes can easily be modeled by straight lines l_i with vectors \vec{x}_{t_i} and vector \vec{x}_d . Vector \vec{x}_d is the same for all straight lines l_i . We get vectors \vec{x}_{t_i} by moving vector \vec{x}_t 2mm to the front/back perpendicular to \vec{x}_d for the anterior/posterior electrode and accordingly 2mm to the right/left perpendicular to \vec{x}_d for the medial/lateral electrode

(depending on the side of the head). For each electrode i of the five electrodes, the distances $d_{i,e}$ for entering STN and $d_{i,a}$ for exiting STN are results of MER labeling and can be measured as distances (in mm) from the target point.

In the case, that we use an analytical and regular 3D surface like an ellipsoid for modeling of the STN, calculation of intersections with electrodes represented by straight lines is achieved in a mathematical straightforward manner. Here, we will consider irregular object surfaces as provided by STN segmentation in T2-MRI. We have chosen an analytical and efficient approach for calculation of the points, where the STN surface and straight lines l_i intersect.

The discrete surface of the STN is built from surfaces of STN voxels which aren't adjacent to a surface of other STN voxels. The voxel surfaces are planes E , which can be described by a base vector \vec{x}_E and direction vectors r_{E1} and r_{E2} :

$$E : \vec{x} = \vec{x}_E + t_1 \cdot r_{E1} + t_2 \cdot r_{E2} \quad . \quad (8)$$

Intersection of a straight line l with plane E is given by solving

$$\vec{x}_E + t_1 \cdot r_{E1} + t_2 \cdot r_{E2} = \vec{x}_t + t \cdot \vec{x}_d \quad . \quad (9)$$

In order to save processing time – a STN consisting of 150 voxels and using 5 electrodes and nearly 24.500 search positions produces approx. 220 million equation systems – we collect all voxel surfaces lying in the same plane. Each voxel surface within this plane is marked in a logical matrix. We collect all the planes (and their logical matrices) showing in the same direction and get a logical 3D matrix. There are 6 logical 3D matrices for 6 directions of the discrete surface of STN. For each direction, intersections of all planes and straight lines of the electrode model are calculated and accepted, if the logical matrix is true for that position.

2.8.2. Estimating electrode position in STN. A measure G is used that compares the measured (by MER labeling) and calculated (by model matching) entry and exit points of electrodes into and out of STN:

$$G = \sum_{i=1}^5 |d_{i,MER-e} - d_{i,calc-e}| + |d_{i,MER-a} - d_{i,calc-a}| \quad . \quad (10)$$

A displacement space is specified according to typical geometric deviations of the stereotactic system. Then, the STN model is systematically shifted over all displacement positions and the resulting entry and exit points are calculated for all electrodes. The displacement position with smallest value for G is selected as best matching between labeled MER data and calculated intersections of electrodes and STN model. This supplies an estimated registration of the actual position of the electrodes related to the target structure. Fig. 4 visualizes a STN model with estimated best matching of intersecting electrodes.

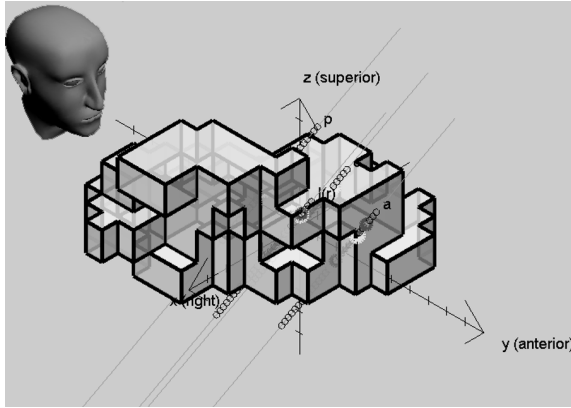


Figure 4. Matching of STN model with intersecting electrodes

3. Results and discussion

Both systems have been developed and implemented as software prototypes with MatlabTM. MER data records of 14 patients were selected randomly from surgery records providing us MERs of 103 electrodes and a total of 2434 recordings. We used a subset of 16 electrodes for system development and the remaining ones for verification. Compared to classification notes from an experienced surgeon, the MER classifier decided correctly for 2078 recordings out of 2200. Recordings (234) without clear assignment by the surgeon were neglected. Thus, nearly 95% of the recordings were classified correctly. Uncertain or wrong decisions mainly occurred with signals recorded near the STN boundary or with such from electrodes, that did not show clear STN signals at all.

The fusion of MER classification with STN segmentation from T2-MRI was tested with data from 6 patients. The system showed stable results when at least labeling from 4 electrodes was available. Further testing is planned with real electrode positions extracted from postoperative CT images.

At present, the structure of the classifier is based on a sequentially ordered means of feature extraction and according decision steps. With minor modifications, the degree of fulfillment of a criterion can be produced in each level. This would reflect the degree to which a signal is neuronal active. For example, we have introduced the extracted features into a common feature space and trained a decision system using a Fuzzy cluster algorithm. The resulting Fuzzy classifier showed at least the same results as the hierarchical one.

There exist other structures (e.g. globus pallidus) which are used as targets for the treatment of Parkinson's disease by DBS. Additionally, the treatment of other diseases like Dystonia is already common practise and other diseases like

psychic illnesses are in a promising focus of research also. Therefore, the need for MER classification grows with expanding diagnosis domains for DBS therapy. Extending the classifier to handle various kinds of signals seems to be a demanding but also promising field to us.

References

- [1] J. K. Krauss, J. Jankovic, and R. G. Grossman. *Surgery for Parkinson's Disease and Movement Disorders*. Lippincott Williams and Wilkins, Philadelphia, 2001.
- [2] C. Hamani, J. A. Saint-Cyr, J. Fraser, M. Kaplitt, and A. M. Lozano. The subthalamic nucleus in the context of movement disorders. *Brain*, 127(1):4–20, Nov. 2003.
- [3] P. Gemmar, F. Hertel, F. Gielen, and P. Appenroth. Method and apparatus for identification of anatomical landmarks. *US Patent Application*, 2006.
- [4] P. V. Theodosopoulos, W. J. Marks, C. Christine, and P. A. Starr. Locations of movement-related cells in the human subthalamic nucleus in parkinson's disease. *Movement Disorders*, 18(7):791–798, 2003.
- [5] A. Benazzouz, S. Breit, A. Koudsie, P. Pollak, P. Krack, and A.-L. Benabid. Intraoperative microrecordings of the subthalamic nucleus in parkinson's disease. *Movement disorders*, 17:145–149, 2002.
- [6] W. D. Hutchison, R. J. Allan, H. OPitz, R. Levy, J. O. Dostrovsky, A. E. Lang, and A. M. Lozano. Neurophysiological identification of the subthalamic nucleus in surgery for parkinson disease. *Annals of Neurology*, 44(4):622–628, 1998.
- [7] J. H. Falkenberg, J. McNames, J. Favre, and K. J. Burchiel. Automatic analysis and data visualization of microelectrode recording trajectories to the subthalamic nucleus: Preliminary results. *Stereotactic and Functional Neurosurgery*, 84(1):35–45, 2006.
- [8] J. McNames. Microelectrode signal analysis techniques for improved localization. In Z. Israel and K.J.Burchiel, editors, *Microelectrode Recordings in Movement Disorder Surgery*, pages 119–129, New York, 2004. Thieme.
- [9] K. Menne and U. Hofmann. Automatic neurophysiological identification of the human subthalamic nucleus for the implantation of deep brain stimulation electrodes based on statistical signal processing methods and unsupervised classification. In *EMBE 2005 - 3rd European Medical & Biological Engineering Conference - IFMBE European Conference on Biomedical Engineering*, pages 1727–1983, Prague, 2005. IFMBE Proceedings ISSN.
- [10] G. Schaltenbrand and W. Wahren. *Atlas for Stereotaxy of the Human Brain*. Thieme, Stuttgart, 92.
- [11] J. Talairach and P. Tournoux. *Co-Planar Stereotaxic Atlas of the Human Brain*. Thieme Medical Publishers, 1998.
- [12] D. L. Donoho. De-noising by soft-thresholding. *IEEE Transactions on Information Theory*, 41(3):613–627, 1995.
- [13] I. Daubechies. *Ten lectures on wavelets*. Society for Industrial and Applied Mathematics, 1992.